From Ligand to Complexes: Inhibition of Human Immunodeficiency Virus Type 1 Integrase by β-Diketo Acid Metal Complexes

Mario Sechi,*,† Alessia Bacchi,‡ Mauro Carcelli,‡ Carlotta Compari,§ Elenia Duce,§ Emilia Fisicaro,§ Dominga Rogolino,‡ Paul Gates,|| Marco Derudas,† Laith Q. Al-Mawsawi,⊥ and Nouri Neamati*,⊥

Dipartimento Farmaco Chimico Tossicologico, Università di Sassari, Via Muroni 23/A, 07100 Sassari, Italy, Dipartimento di Chimica Generale ed Inorganica, Chimica Analitica, Chimica Fisica, and Dipartimento di Scienze Farmacologiche, Biologiche e Chimiche Applicate, Università di Parma, Parco Area delle Scienze 17/A, 43100 Parma, Italy, School of Chemistry, University of Bristol, Cantok's Close, Bristol BS8 1TS, United Kingdom, and Department of Pharmaceutical Sciences, School of Pharmacy, University of Southern California, 1985 Zonal Avenue, PSC 304, Los Angeles, California 90089

Received February 18, 2006

β-Diketo acid-containing compounds are a promising class of human immunodeficiency virus type 1 (HIV-1) integrase (IN) inhibitors. Starting from the hypothesis that these inhibitors are able to coordinate ions in solution before interacting on the active site, a series of potentiometric measurements have been performed to understand the coordination ability of the diketo acid pharmacophore toward the biologically relevant Mg^{2+}. Moreover, by using β-diketo acid/ester as model ligands with a set of divalent metal ions (Mg, Mn, Ni, Co, Cu, and Zn), we obtained a series of complexes and tested them for anti-HIV-1 IN activity. Results demonstrate that the diketo acid functionality chelates divalent metal ions in solution, and complexes with metals in different stoichiometric ratios are isolated. We postulate that the diketo acids act as complexes in their active form. In particular, they predominantly form species such as Mg_2L^{2+} and Mg_2L_2 (derived from diketo acids, H_2L), and MgL^+ and MgL_2 (derived from diketo esters, HL) at physiological pH. Furthermore, the synthesized mono- and dimetallic complexes inhibited IN at a high nanomolar to low micromolar range, with metal dependency in the phenyl diketo acid series. Retrospective analysis suggests that the electronic properties of the aromatic framework influence the metal-chelating ability of the diketo acid system. Therefore, the difference in activities is related to the complexes they preferentially form in solution, and these findings are important for the design of a new generation of IN inhibitors.

Introduction

Human immunodeficiency virus type 1 (HIV-1) integrase (IN) is an attractive and validated target for developing novel antiretroviral agents.[1−9] Because of its vital role in the viral replication cycle, with no human counterpart of the enzyme known, the addition of an IN inhibitor to existing components of antiretroviral therapy[10−13] is expected to improve the outcome of therapy by potential synergism, without exacerbating toxicity issues.

The integration process is catalyzed by IN through two different reactions: 3′-processing and strand transfer.[14−16] Following reverse transcription, the viral cDNA is primed for integration in the cytoplasm by endonucleolytic cleavage of the 3′ viral DNA ends by removing the last two nucleotides (GT). This step is referred to as the 3′-processing reaction and generates two CA-3′-hydroxyl recessed ends, which are the reactive intermediates required for the next step, strand transfer. After 3′-processing, IN remains bound to the viral cDNA as a multimeric complex that bridges both ends of the viral DNA within intracellular particles called preintegration complexes. The preintegration complex then translocates into the nucleus, where IN catalyzes joining of the processed 3′-OH DNA ends to the 5′-DNA phosphate of the host chromosome (strand transfer reaction). Viral integration is completed by the removal of unpaired nucleotides and gap repair, carried out by cellular enzymes, leading to stable provirus formation.

HIV-1 IN belongs to a large family of polynucleotidyl transferases that include transposases and polymerases[17−19] and is composed of a single polypeptide chain of 288 aa that folds into three functional domains. The catalytic core domain comprises residues 51−212 and contains the D,D(35)E motif, two aspartates (D64 and D116) and one glutamate (E152), which are essential for enzymatic activity.[20,21] The conservation of this catalytic triad extends beyond retroviral integrases, as retrotransposons and some prokaryotic transposases contain the same arrangement of catalytically essential carboxylates. These amino acid residues coordinate divalent metal ions such as Mg^{2+} or Mn^{2+}, perhaps as a "two-metal-ion" mechanism, similar to other polynucleotide polymerases.[17,22−24] As revealed from available X-ray structures of the HIV-1 IN core domain, the two aspartate residues (D64 and D116) form a coordination complex with Mg^{2+}.[21] It has been proposed that a second metal can be most likely coordinated by E152 (with either D116 or D64) once HIV-1 IN binds its DNA substrate.[25,26] Additionally, it has been hypothesized that the two metal ions need not be present at the active site of IN throughout its entire enzymatic reaction. In this sequential metal dependency view, the first metal ion, bound to the two aspartates, could play a major role in the 3′-processing reaction, whereas the second one, bound prevalently to the glutamate, may be more relevant during the strand transfer reaction.[27,28] It is therefore likely that the metal cofactor(s) coordinate(s) IN with the phosphodiester backbone of the DNA substrate(s) during the 3′-processing and strand transfer steps.

* To whom correspondence should be addressed: (M.S.) tel +39 079-228-753, fax +39 079-228-720, e-mail mario.sechi@uniss.it; (N.N.) tel +1 323-442-2341, fax +1 323-442-1390, e-mail neamati@usc.edu.

† Università di Sassari.

‡ Dipartimento di Chimica Generale ed Inorganica, Chimica Analitica, Chimica Fisica, Università di Parma.

§ Dipartimento di Scienze Farmacologiche, Biologiche e Chimiche Applicate, Università di Parma.

|| University of Bristol.

⊥ University of Southern California.

10.1021/jm060193m CCC: $33.50 © 2006 American Chemical Society
Published on Web 06/20/2006

Chart 1. Structures of Representative β-Diketo-Based Inhibitors

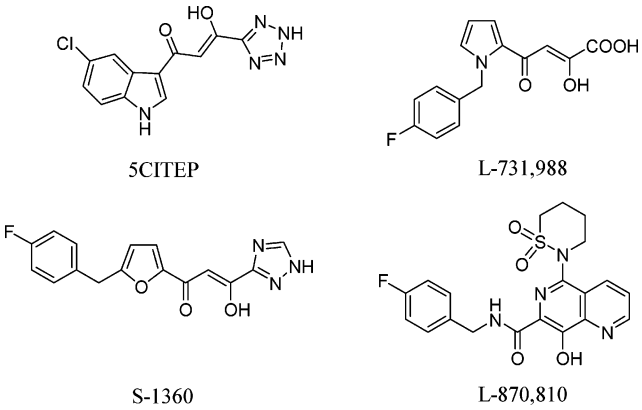

In most structures, the catalytic core domain contains a short disordered loop (encompassing residues 141−150) that can be stabilized by DNA.[13]

In the past several years, a plethora of compounds with diverse structural features have been reported as IN inhibitors.[13,29−33] Several of them inhibit both the viral enzyme and viral replication in cell-based assays as well as in animal models. However, as of today, no inhibitor of HIV-1 IN has been approved. Recently, a class of compounds bearing a β-diketo acid moiety, independently discovered by scientists from Shionogi & Co. Ltd. and Merck Research Laboratories, have emerged as the most promising lead in anti-HIV-1 IN drug discovery.[34] A diketo acid bioisosteric analogue, 5CITEP (Chart 1), was subsequently cocrystallized with the enzyme, providing the first X-ray crystal structure of an inhibitor in complex with HIV-1 IN.[35] Meanwhile, other members of the diketo acid family, exemplified by L-731,988 (Chart 1), have been reported[36,37] and intensively studied.[38−41] Several diketo acid congeners selectively inhibit the strand transfer reaction, and in cell-based assays they inhibit integration without affecting earlier phases of the HIV-1 replication cycle.[36,42] Until now only two compounds, the Shionogi/Glaxo-SmithKline's (S/GSK) S-1360[43,44] and Merck's L-870,810[45,46] (Chart 1), both belonging to this class of compounds, have entered clinical trials.[33] However, due to pharmacokinetic problems, S/GSK decided to end the development of S-1360.[47] Although several synthetic and biological studies for diketo acid compounds have been reported, the mechanism by which they bind IN has not been well understood. It is believed that the β-diketo acid pharmacophoric motif could be involved in a functional sequestration of one or both divalent metal ions (Figure 1a), which are critical cofactors at the enzyme catalytic site.[25] This would subsequently block the transition state of the IN−DNA complex.[13,42] In this scenario, it is of paramount importance to acquire information about the mode of action of diketo acids, which could then be useful in the design of new compounds as IN inhibitors.

With this aim, we investigated some features of diketo acid-containing compounds that might be correlated with their mechanism of action. In particular, we verified the complexing ability of the diketo acid motif for divalent metal ions, starting from the insight that they could coordinate ions in solution before interaction at their putative binding site. Structural evidence indicates the possible ion complexation of diketo acid compounds with metals of biological interest, such as magnesium and manganese. In particular, β-diketo acids (H_2L, Figure 1b) present two binding sites that can be involved in coordination and the possibility to give complexes with different metals with defined stoichiometry. Instead, β-diketo esters (HL, Figure 1b) can provide only the keto−enol function to be used in coordination.

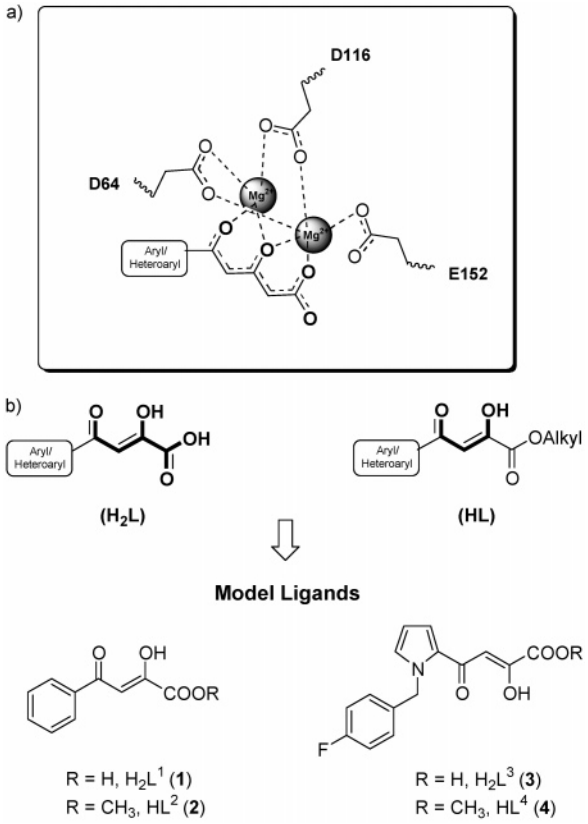

Figure 1. (a) Proposed chelating mechanism for β-diketo acids in enzyme active site. (b) Complexing motif for β-diketo acid/esters and model ligands used in this study.

This rationale is also supported by considering the intracellular and assay concentrations of metal cofactors required for catalysis. It is generally accepted that Mg^{2+} is a more reasonable cofactor for integration in cells,[48] while Mn^{2+} appears to be preferred in vitro.[25,49,50] IN specific activities are at least 10-fold higher with Mn^{2+} versus Mg^{2+} under similar conditions. Concentrations of these ions are $\sim 10^{-7}$ M for Mg^{2+} ($< 10^{-7}$ M for Mn^{2+}) in cells and 7.5 mM for Mn^{2+} in IN inhibition assays.[51−54] Because these concentrations are higher than the number of IN molecules (40−100 IN molecules are packaged within each HIV virion), the formation of complexes in solution is favored.

Therefore, to identify some of the hypothesized complexes in solution, a series of potentiometric measurements were conducted for two diketo acids [(2*Z*)-2-hydroxy-4-oxo-4-phenylbut-2-enoic acid (**1**), H_2L^1, and (2*Z*)-4-[1-(4-fluorobenzyl)-1*H*-pyrrol-2-yl]-2-hydroxy-4-oxobut-2-enoic acid (**3**), H_2L^3] and their respective methyl esters (**2**, HL^2, and **4**, HL^4) in the presence of magnesium ions under various experimental conditions. According to our analysis, several species and solution equilibria for both diketo acids and diketo esters are present. These observations allowed us to synthesize new complex-based inhibitors, which constituted our second goal. Thus, by using the same model ligands and Mg, Mn, Ni, Co, Cu, and Zn divalent ions, we obtained the complexes **9a**−**f**, **10**, **11a**−**f**, **12**, and **13** (Scheme 2), which have been characterized by means of IR and NMR spectroscopy, mass spectrometry (electrospray ionization, ESI, and fast atom bombardment, FAB), and elemental analysis. We further tested them for anti-HIV-1 IN activity. Additionally, we confirmed the structure of ligand H_2L^3 (L-731,988) by X-ray crystallographic analysis. Moreover,

Scheme 1. Preparation of Diketo Ligands[a]

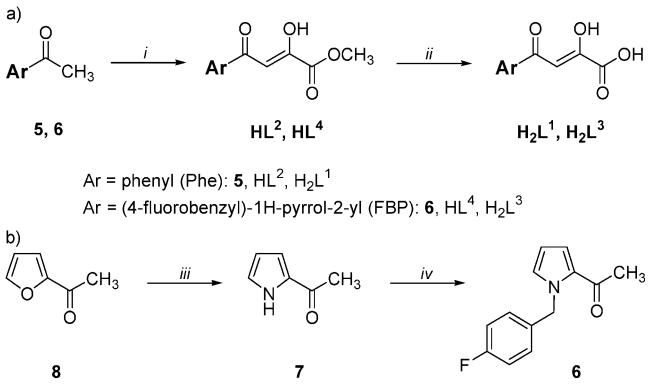

[a] Reagents and conditions: (a) (i) dimethyloxalate, NaH, DMF, room temperature (rt) for 3.5 h, next 50 °C for 1 h; (ii) 2 N NaOH, methanol, rt for 5 h, then 1 N HCl. (b) (iii) 30% NH_3, ethanol, sealed tube, 150 °C for 12 h; (iv) KOH pellets, DMSO, rt for 45 min, then 4-fluorobenzylbromide, 50 °C for 45 min.

enzyme assays were also undertaken to investigate the role of the simple ligands and/or of the related complexes in the presence of different metals for IN inhibition. Analysis of these results persuaded us to propose a potential mechanism of action for the diketo acid family of IN inhibitors, which is herein detailed.

Results and Discussion

Preparation of the Ligands. The synthetic approach for the preparation of diketo ligands H_2L^1, HL^2, H_2L^3, and HL^4, chosen as model compounds, is depicted in Scheme 1. In particular, the β-diketo acids H_2L^1 and H_2L^3 were obtained by alkaline hydrolysis from their respective β-diketo esters HL^2 and HL^4. The latter were synthesized by Claisen condensation of the appropriate acetyl derivatives **5** and **6** with dimethyloxalate in the presence of sodium hydride in anhydrous *N*,*N*-dimethylformamide (DMF) by following a known procedure[55] (Scheme 1a). While the acetophenone **5** was commercially available, the intermediate **6** was easily obtained by adapting a method previously reported by our group.[56] Pyrrolization of 2-acetylfuran **8** with 30% NH_3 in a sealed tube at 160 °C afforded the intermediate **7** in good yield. Alkylation of the 2-acetylpyrrole **7** with 4-fluorobenzylbromide in powdered KOH/dimethyl sulfoxide (DMSO) gave the corresponding alkylpyrrole **6** (Scheme 1b).

All ligands were prevalently in keto−enolic form in solution, with a small amount of their diketonic tautomers (5−8%). Analysis of ^{1}H NMR spectra, recorded in $CDCl_3$, in DMSO-d_6, and in a 3:1 mixture, revealed the presence of C-*H* protons downfield in a 6.80−6.90 ppm resonance range, indicating the enolic form. For diketo acids H_2L^1 and H_2L^3 the coexistence of both the enolic and ketonic tautomers was observed, while this was less evident for the diketo ester HL^2. In particular, small singlets for CH_2 protons were revealed at ∼4.3−4.6 ppm. Because of overlap with other signals, a full characterization of the keto tautomers remains unclear. Otherwise, only enolic protons were detectable for the diketo ester HL^4. Furthermore, due to exchangeable enolic hydrogens, all ligands showed a broad singlet in the 12−15 ppm region. These observations were further confirmed by ^{13}C NMR and distortionless enhancement by polarization transfer (DEPT), which were carried out for all the ligands. In fact, spectra recorded in DMSO-d_6 showed clear *C*H enolic carbons at about 100 ppm. Meanwhile, signals corresponding to *C*H_2 carbons for H_2L^1, HL^2, and H_2L^3 in their diketo form were observed in the 48−52 ppm range, in agreement with reports by Maurin et al.[57] The solution structures of several β-diketo acids by means of ^{1}H- and ^{13}C NMR experiments were also studied by Brecker et al.[58] They observed that 4-aryl-β-diketo acids form predominantly a more energetically favorable enol structure at the 2-keto group when dissolved in aprotic solvents. Also, it is noteworthy that β-diketo acids bearing 4-aryl substituents gave, in aqueous solution, one pH-independent isomer formulated with a delocalized π-electron system on the carbon atoms in 2-, 3-, and 4-positions in conjugation with the arene in C-4. Possibly due to an interconversion between the two formal enolate structures, 4-aryl-β-diketo acids could presumably constitute a pseudodienolate system at pH 7.5. However, these analyses confirmed the presence of a keto−enolic structure, which is predicted to be an important structural feature for complexation.

X-ray Crystallography. Figure 2 and Tables 1 and 2 report the structural details of H_2L^3. In analogy with our recent work,[41] the X-ray crystallographic data of compound H_2L^3 indicate that the enolic bond is situated in the 2,3 position with respect to the carboxylic group [C−C = 1.464(7)/1.463(7) Å and C=C = 1.339(6)/1.347(6) Å, respectively, for the two independent molecules]. The keto−enolic resonance stabilizes the associated intramolecular hydrogen bonds, which show similar geometry in the two independent molecules [O2−H···O1 = 2.546(6) Å and 150(5)°; O6−H···O5 = 2.540(6) Å and 155(8)°]. A pair of intermolecular hydrogen bonds of similar remarkable strength determines the pairing of the independent molecules through the carboxylic dimer pattern [O3−H···O7 = 2.654(6) Å and 170(8)°; O8−H···O4 = 2.682(6)Å and 156(6)°]. The dimer is pseudo-centrosymmetric and presents an overall Z-shape, composed by a planar central skeleton comprising the pyrrolic rings, the keto−enolic systems, and the intermolecular carboxylic acids dimer (maximum deviation from the average plane = 0.2 Å) (Figure 2a). This is flanked by two almost perpendicular wings, constituted by the terminal *p*-fluoroaryl substituents, in trans; they form dihedral angles of 87° and 80° with the rigid planar molecular core. The dimers stack in the crystal with a separation of 3.2 Å among the planar cores, so that each fluorine atom lies 3.5 Å above the center of an adjacent fluoroaryl ring (Figure 2b).

Potentiometric Measurement and Calculations. The equilibrium constants of the ligands H_2L^1, HL^2, H_2L^3 and HL^4 and the speciation models for Mg^{2+} complexes were studied by potentiometric titrations; the results are reported in Table 3 and Figure 3. To avoid solubility problems, all the titrations were carried out in methanol/water = 9/1 (v/v), where the species are soluble. Only the system HL^2/Mg^{2+} gives rise, at high pH, to a white precipitate that, after some time, dissolves. This precipitate is perhaps a magnesium complex that successively dissolves because of the basic hydrolysis of the ester group of the ligand. First, the protonation constants of the ligands are determined: H_2L^1 is more acid than H_2L^3 [pK_{a1} = 3.81(4) and pK_{a2} = 9.89(3); pK_{a1} = 4.25(5) and pK_{a2} = 11.66(3), for H_2L^1 and H_2L^3, respectively]; the same results for the esters HL^2 and HL^4 [pK_a = 7.64(3) and 8.94(6), respectively]. Then, the stoichiometry of the magnesium(II) complexes and their formation constants are investigated. In the solutions with H_2L^1 or H_2L^3 and Mg^{2+}, the best statistical parameters for the fit are obtained by using the same set of species, MgL_2^{2-}, Mg_2L^{2+}, Mg_2L_2, and, at pH >11, $Mg_2L_2(OH)^-$, but the cumulative formation constants differ significantly (Table 3). In particular, at physiological pH the species Mg_2L^{2+} is predominant with H_2L^1 (Figure 3a), whereas with H_2L^3 this species is only 10% and Mg_2L_2 is the most abundant one (Figure 3c). The reason

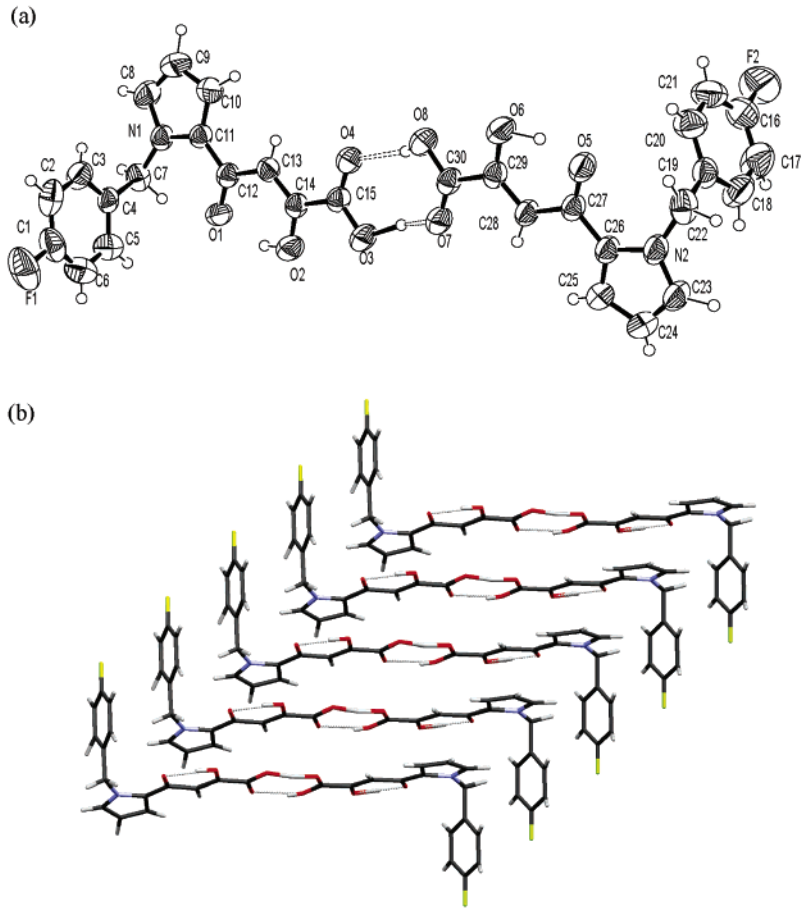

Figure 2. (a) Perspective view and atomic numbering of the two independent molecules of H_2L^3 in the crystal structure, forming a hydrogen-bonded dimer. Thermal ellipsoids are represented at the 50% level. (b) Crystal associations of hydrogen-bonded dimers in H_2L^3.

Table 1. Crystal Data and Structure Refinement for H_2L^3

empirical formula	$C_{15}H_{12}FNO_4$
formula weight	289.26
temperature	293(2) K
wavelength	1.54178 Å
crystal system	monoclinic
space group	*P*21
unit cell dimensions	$a = 4.763(1)$ Å
	$b = 19.027(1)$ Å
	$c = 15.085(1)$ Å
	$\beta = 94.97(1)°$
volume	1361.9(3) Å^3
Z	4
density (calcd)	1.411 Mg/m^3
absorption coefficient	0.953 mm^{-1}
F(000)	600
θ range for data collection	3.75°−70.0°
reflns collected	2751
independent reflns	2732 [*R*(int) = 0.0866]
refinement method	full-matrix least-squares on F^2
data/restraints/parameters	2732/1/472
goodness-of-fit on F^2	0.997
final *R* indices [$I > 2\sigma(I)$]	$R1 = 0.0546$, w$R2 = 0.1497$
R indices (all data)	$R1 = 0.0725$, w$R2 = 0.1673$
absolute structure parameter	0.2(3)
extinction coefficient	0.0029(10)
largest ΔF max/min	0.213/−0.230 e·Å^{-3}

Table 2. Most Relevant Bond Lengths and Angles for H_2L^3

bond	length[a] (Å)	bond	length[a] (Å)
O(1)−C(12)	1.251(6)	O(5)−C(27)	1.242(6)
O(2)−C(14)	1.329(6)	O(6)−C(29)	1.328(6)
O(3)−C(15)	1.305(6)	O(8)−C(30)	1.300(6)
O(4)−C(15)	1.233(6)	O(7)−C(30)	1.223(6)
C(12)−C(13)	1.464(7)	C(27)−C(28)	1.463(7)
C(13)−C(14)	1.339(6)	C(28)−C(29)	1.347(6)
C(14)−C(15)	1.482(6)	C(29)−C(30)	1.509(7)
	angle[a] (deg)		angle[a] (deg)
O(1)−C(12)−C(13)	118.4(4)	O(5)−C(27)−C(28)	119.7(4)
C(14)−C(13)−C(12)	121.4(5)	C(29)−C(28)−C(27)	120.0(5)
O(2)−C(14)−C(13)	124.5(4)	O(6)−C(29)−C(28)	124.8(5)

[a] Shown in parentheses are the su values.

may be partly related to the greater steric hindrance of the aryl residue in H_2L^3, disfavoring the simultaneous interaction of two metal ions with the same ligand molecule. To verify the formation of polymetal M_2L_2 compounds in solution, we have done titrations at the same ligand:metal *ratio* but at different concentrations. The nonoverlapping of the titration curves supports the hypothesis of the presence of polymetal complexes.[59] Complex species with the monoprotonated ligand HL^- were rejected during the refinement. The formation constants of the monomer MgL and of the dimer Mg_2L_2 cannot be refined together, probably because of the high mathematical correlation between the two species. By means of potentiometry alone, we cannot completely reject the hypothesis of the formation of monomeric species, because the model with ML instead of M_2L_2 is only slightly unfavorable. The preference for Mg_2L_2 over MgL, besides the better statistical values, is discussed with the spectroscopic characterization of the synthesized complexes (see below).

As far as the equilibria between the esters HL^2 and HL^4 and magnesium ions are concerned, the set of species giving rise to the best fit is formed by MgL^+ and MgL_2. At physiological pH, the two complexes are present approximately in equimolar

Table 3. Logarithms of Protonation and Mg(II)−Complex Formation Constants[a]

	p	*q*	*r*	H_2L^1 (**1**)	H_2L^3 (**3**)	HL^2 (**2**)	HL^4 (**4**)
L + H ⇌ LH	0	1	1	9.89 (0.02)	11.66 (0.03)	7.64 (0.03)	8.94 (0.06)
L + 2H ⇌ LH_2	0	1	2	13.70 (0.04)	15.91 (0.06)		
Mg + L ⇌ MgL	1	1	0			5.11 (0.02)	7.16 (0.10)
Mg + 2L ⇌ MgL_2	1	2	0	8.81 (0.30)	12.45 (0.26)	8.86 (0.08)	11.77 (0.40)
2Mg + L ⇌ Mg_2L	2	1	0	9.43 (0.17)	10.46 (0.16)		
Mg + 2L ⇌ Mg_2Cl_2	2	2	−0	14.14 (0.25)	17.99 (0.10)		
2Mg + 2 L + OH ⇌ Mg_2L_2 (OH)	2	2	−1	3.89 (0.18)	7.80 (0.10)		

[a] $\beta pqr = [Mg_pL_qH_r]/[Mg]^p[L]^q[H]^r$. Constants were measured in methanol/water = 9:1 (v/v), I = 0.1 M KCl at 25 °C for the ligands under study. Standard deviations are given in parentheses. Charges are omitted for simplicity.

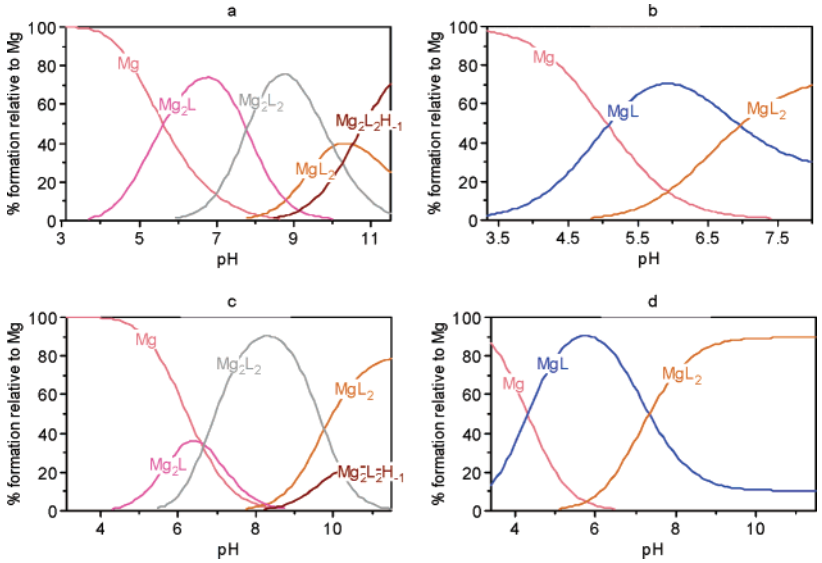

Figure 3. Distribution diagrams for the systems under investigation at L:Mg = 2:1 (concentration of the ligand is 4 mM): (a) L = H_2L^1, (b) L = HL^2, (c) L = H_2L^3, and (d) L = HL^4.

Scheme 2. Preparation of Complexes **9a**−**f**, **11a**−**f**, and **13**[a]

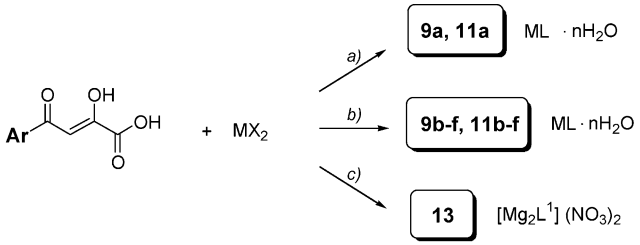

9, 13: Ar = Phenyl (Phe)
11: Ar = (4-fluorobenzyl)-1H-pyrrol-2-yl (FBP)

M = Divalent metal: **a** = Mg(II), **b** = Mn(II), **c** = Ni(II), **d** = Co(II), **e** = Cu(II), **f** = Zn(II)
X = hydroxide, acetate or nitrate

[a] Reagents and conditions: (a) methanol, $Mg(OH)_2$ suspension in water, room temperature (rt), overnight; (b) methanol, aqueous solution of the appropriate acetate salt, rt; (c) methanol, 0.1 M NaOH until pH 7, $Mg(NO_3)_2$, rt, 2 h.

ratio. A distribution diagram for both ligands is reported in Figure 3b,d for the ligand-to-metal ratio of 2:1.

Synthesis and Characterization of the Complexes. A schematic representation of complexes **9a**−**f**, **10**, **11a**−**f**, **12**, and **13** is shown in Schemes 2 and 3.

A new series of metal complexes of the diketo acid ligands H_2L^1 and H_2L^3 and Mg(II), Mn(II), Ni(II), Co(II), Cu(II), and Zn(II) have been synthesized and fully characterized. The two molecules show analogous ligand behavior, the functional groups being the same. For Mn(II), Ni(II), Co(II), Cu(II), and Zn(II), the use of acetate salts is sufficient to induce the deprotonation of the ligands, and the corresponding complexes

Scheme 3. Preparation of Complexes **10** and **12**[a]

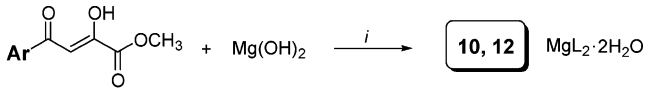

Ar = Phenyl (Phe): **10**
Ar = (4-fluorobenzyl)-1H-pyrrol-2-yl (FBP): **12**

[a] Reagents and conditions: (i) methanol, $Mg(OH)_2$ in aqueous solution, room temperature, then 1 h (for **10**) or 2 h (for **12**).

9b−**f** and **11b**−**f** of general formula ML·xH_2O (x = 0.5−4) can be easily isolated from the reaction medium as insoluble powders (Scheme 2). Concerning the magnesium complexes **9a** and **11a**, the hydroxide is the reagent of choice to ensure the deprotonation of the ligand and the consequent isolation of the 1:1 metal to ligand complex (Scheme 2). The complete deprotonation of the ligands and the coordination of the diketo acid moiety to the metal can be inferred through the IR spectra of the complexes. These spectra are similar: the OH absorption disappears (2650−3100 cm^{-1} in the free ligands), and the C=O bands shift from 1735 to 1660−1570 cm^{-1} for the H_2L^1 complexes and from 1707 cm^{-1} to about 1580 cm^{-1} for the H_2L^3 complexes. A broad absorption at about 3400 cm^{-1} indicates the presence of water molecules in the coordination sphere.

The paramagnetic nature of the Mn, Ni, Co, and Cu complexes prevents the registration of the ^1H NMR spectra. For MgL^1, MgL^3, and ZnL^1, the protonic spectra in CD_3OD confirm the deprotonation of the ligand: the signals of the acidic protons are in fact absent in all cases. The chemical shifts for these complexes show a 0.15−0.20 ppm downfield shift of all the signals versus the free ligands. Elemental analysis and mass data confirm the proposed 1:1 stoichiometry.

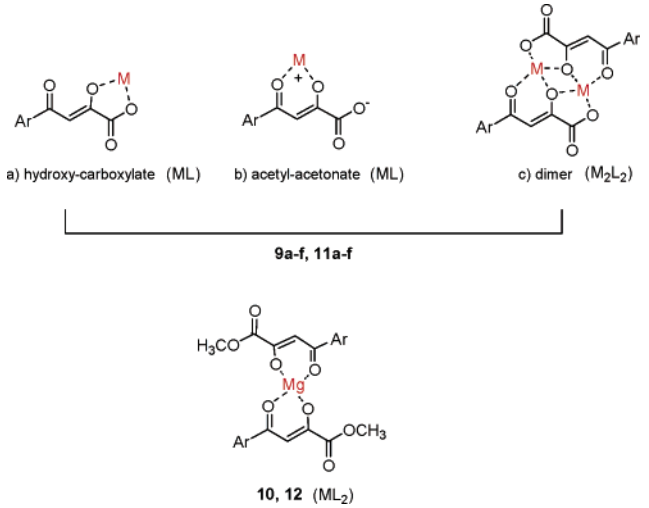

Figure 4. Structural hypothesis for the synthesized complexes.

H_2L^1 and H_2L^3 can coordinate in the hydroxy-carboxylate form (Figure 4a), as determined by X-ray diffraction analysis in the crystal structure of [bis(ethylenediamine)acetylpyruvato]-cobalt(III) iodide,[60] or in the acetyl-acetonate form (Figure 4b), as found in the crystal structure of (1*R*,2*R*-cyclohexanediamine-*N*,*N*′)[2-hydroxy-4-oxo-2-pentenoato]platinum(II).[61] In the IR spectra of our complexes, the band of a free C═O is absent, so it is possible to exclude that the ligand is in the hydroxy-carboxylate form. Moreover, some mass data and the work of Cotelle and co-workers[62] suggest the presence of M_2L_2 species, where both the binding modes of the ligand are used to give a dimer (Figure 4c) (or, eventually, a polymer). Also in this case there are no free C═O groups in the structure. In all the cases the coordination sphere of the metals is completed by water molecules. The potentiometric measurements (see above) are in line with the hypothesis of a dimeric structure. At this stage, the more reasonable structural hypothesis for these complexes considers that the acetyl, the hydroxyl, and the carboxylate groups coordinate to the metal.

With the aim to confirm the presence of the complex $[Mg_2L^1]^{2+}$, which is the predominant species at physiological pH according to potentiometric measurement (see above), H_2L^1 has been deprotonated with NaOH and subsequently reacted with magnesium nitrate. A white, highly hygroscopic powder was isolated, which corresponds to $[Mg_2L^1](NO_3)_2$ (**13**). The hygroscopic nature of the compound prevents elemental analysis, but the presence of a nitrate group can be inferred by the IR spectrum, with a strong absorption at 1345 cm^{-1}. The ^1H spectrum in CD_3OD indicates a complete deprotonation of the ligand upon coordination. This proposed stoichiometry was confirmed by ESI-mass analysis.

Magnesium complexes of the methyl esters HL^2 and HL^4 were obtained by reacting the metal hydroxide with a methanolic solution of the ligands at room temperature. The corresponding complexes **10** and **12**, with the general formula $MgL_2 \cdot 2H_2O$, can be isolated as air-stable white powders (Scheme 3). As before, the deprotonation of the ligands can be inferred from the IR spectra because of the disappearance of OH absorption (2700−2800 cm^{-1} in the free ligands); a strong band at around 3400 cm^{-1} clearly indicates the presence of water molecules in the coordination sphere of the metal. Upon coordination, the ketonic carbonyl group absorption shifts to 1615−1593 cm^{-1} (1631−1623 cm^{-1} in the free ligands), while the bands of the ester moieties do not show any variation, indicating the exclusion of this group from the coordination. In the ^1H NMR spectra of both **10** and **12**, no remarkable modifications are present versus the free ligands, but only a 0.15−0.20 downfield shift of the signals is observed. Elemental analysis and mass data confirm the proposed 2:1 ligand-to-metal ratio for both the complexes. The two β-diketo esters coordinate the magnesium ion through the diketonic moieties (Figure 4), and the coordination sphere of the metal is completed by two water molecules.

Inhibition of HIV-1 IN. All ligands (H_2L^1, HL^2, H_2L^3, and HL^4) and complexes **9**−**13** were tested for their ability to inhibit IN catalytic activity in in vitro assays employing purified enzyme. Inhibition of IN catalytic activities, 3′-processing (3′-proc) and strand transfer (ST), were evaluated by oligonucleotide-based assays (Figure 5a), and the results are reported in Table 4. With the exception of **10**, all tested complexes showed anti-IN activity in nanomolar/micromolar concentration ranges, with more potency exhibited toward the catalyzed strand transfer process ($IC_{50s} = 0.26 \pm 0.04$ to 44 ± 3 μM) versus 3′-processing as evidenced by their selectivity indexes. The ligands differ in activities as previously reported, thus confirming that the nature of the aromatic ring significantly influences the inhibition potency. This behavior was generally translated to their complexes. Complexes **9a**−**f** displayed inhibitory activities for ST at IC_{50} values at the 5−44 μM (and 26 → 333 μM for 3′-proc) range. Interestingly, these compounds exhibited a certain metal inhibition dependency when tested against IN (for a representative gel, see Figure 5b). For example, while complexes **9a**−**c**, where ligand H_2L^1 is complexed with Mg^{2+}, Mn^{2+}, and Ni^{2+}, respectively, inhibited ST at an IC_{50} value range of 31−44 μM, for complexes **9d**−**f** (M = Co^{2+}, Cu^{2+}, and Zn^{2+}) an increase in potency was observed. In particular, with IC_{50} values of 5 ± 3 and 50 ± 9 μM (ST and 3′-proc), complex **9d** showed the best inhibition profile in the Phe (**9**) series; however, also **9e** and **9f** displayed good inhibitory activities, with IC_{50} values of 11 and 21 μM and 26 and 88 μM (ST and 3′-proc), respectively.

As far as the complexes of H_2L^3 are concerned, IC_{50} values ranged from 0.26 to 0.99 μM and from 6 to 9 μM for ST and 3′-proc, respectively. The complexes **11a**−**f** shared potency comparable to that of the free ligand. The complex MgL^3 (**11a**, $IC_{50} = 0.26 \pm 0.04$ and 6 ± 1 μM for ST and 3′-proc) proved to be the most active tested compound, with 2-fold greater potency than its free ligand. Compared to the **9a**−**f** series, the presence of different metals in the complexes of series **11** did not lead to any significant influence in activity, although a minor decrease in potency was observed.

Inhibition activities for diketo esters HL^2 and HL^4 reflected the results observed for the parent acids. In fact, while HL^2 and its complex **10** were not active for IN inhibition, **12** resulted in a 6-fold increase in potency compared to the free ester ligand HL^4 for strand transfer inhibition, 3′-processing being the same [48 ± 4 and 8 ± 1 μM (ST); 187 ± 6 and 203 ± 22 μM (3′-proc)].

Moreover, to decipher whether the increase in potency of complexes **9c**−**f** with "soft" metal coordination was the result of free metal alone or in conjunction with the organic scaffold of H_2L^1, we performed additional experiments to determine whether the inhibition of purified IN by compound H_2L^1 was positively influenced by the addition of exogenous metals such as Ni^{2+}, Co^{2+}, Cu^{2+}, and Zn^{2+} (Table 5, Figure 6). Results show that both the metal and the organic scaffold are important. Strand transfer inhibition values of H_2L^1 within each metal category (IC_{50} value range of 40−84 μM) are more similar to that of H_2L^1 with no exogenous metal (Table 6). 3′-Processing inhibi-

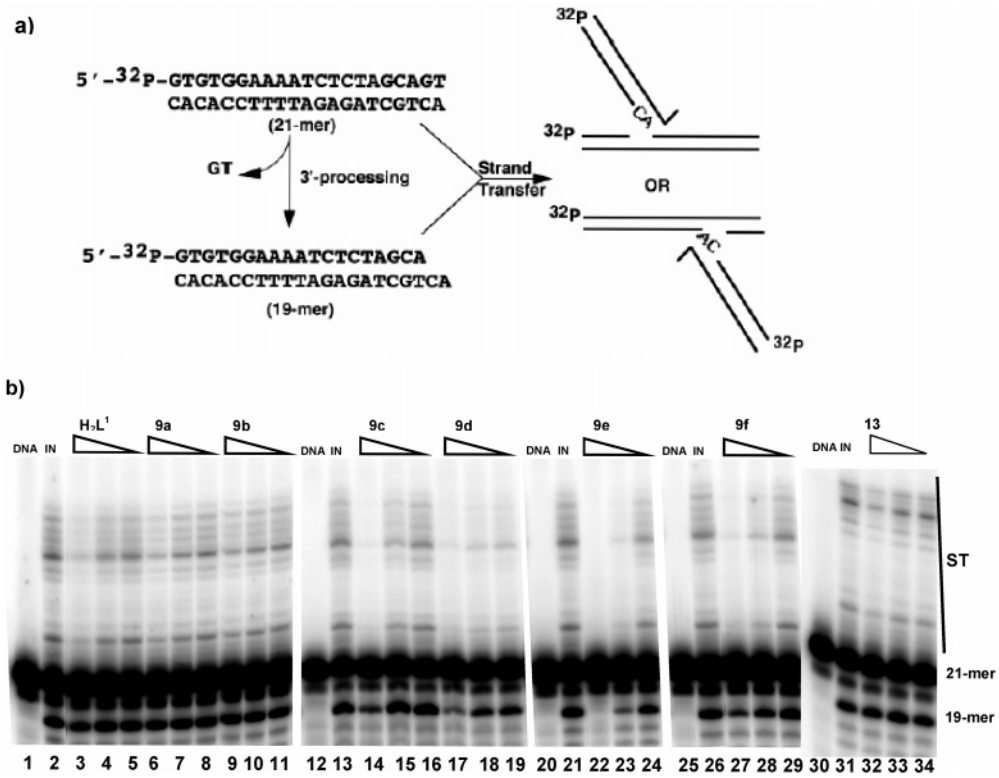

Figure 5. Representative gel showing inhibition of purified IN by selected compounds H_2L^1, **9a**−**f**, and **13**. (a) A 21-mer blunt-end oligonucleotide corresponding to the U5 end of the HIV-1 LTR, 5′ end-labeled with ^{32}P, is reacted with purified IN. The initial step involves nucleolytic cleavage of two bases from the 3′-end, resulting in a 19-mer oligonucleotide. Subsequently, 3′ ends are covalently joined at several sites to another identical oligonucleotide that serves as the target DNA. This reaction is referred to as strand transfer, and the products formed migrate more slowly than the original substrate (shown in the figure as ST for strand transfer products). (b) Lanes 1, 12, 20, 25, and 30, DNA alone; lanes 2, 13, 21, 26, and 31, IN and DNA with no drug; other lanes, IN, DNA, and selected drug concentrations as indicated above each lane. All inhibitor concentrations decrease from 100 μM → 33 μM → 11 μM.

Table 4. Inhibition of HIV-1 IN Catalytic Activities of Ligands and Complexes

compd	M	3′-processing IC_{50} (μM)	strand transfer IC_{50} (μM)	SI[a]
H_2L^1		>333	69 ± 4	>5
HL^2		>333	>333	
H_3L^3		15 ± 2	0.54 ± 0.08	28
HL^4		187 ± 6	48 ± 4	4
9a	Mg^{2+}	>333	44 ± 3	>8
9b	Mn^{2+}	>333	42 ± 4	>8
9c	Ni^{2+}	66 ± 5	31 ± 2	2
9d	Co^{2+}	50 ± 9	5 ± 3	10
9e	Cu^{2+}	26 ± 5	11 ± 3	2
9f	Zn^{2+}	88 ± 10	21 ± 5	4
10	Mg^{2+}	>333	>333	
11a	Mg^{2+}	6 ± 1	0.26 ± 0.04	23
11b	Mn^{2+}	7 ± 1	0.99 ± 0.62	7
11c	Ni^{2+}	6 ± 3	0.52 ± 0.24	11
11d	Co^{2+}	9 ± 4	0.72 ± 0.33	12
11e	Cu^{2+}	6 ± 2	0.62 ± 0.34	10
11f	Zn^{2+}	6 ± 3	0.74 ± 0.43	8
12	Mg^{2+}	203 ± 32	8 ± 1	25
13	Mg^{2+}	>333	88 ± 5	>4

[a] SI = selectivity index.

tion values of H_2L^1 with exogenous Ni^{2+}, Cu^{2+}, and Zn^{2+} (IC_{50} value range of 235 → 333 μM) were also similar to that of H_2L^1 with no exogenous metal. Interestingly, inhibitory results of compound H_2L^1 in the presence of exogenous Co(II) showed a dramatic increase in potency for the 3′-processing catalytic reaction, with an IC_{50} value of 85 μM. This value is similar to that observed for complex **9d**, for which a partial formation of this species could be considered. These results enforced the observation that complexes were sufficiently stable in solution, as suggested from their log β values, supporting a view that they could plausibly act in these forms.

Table 5. Inhibition of HIV-1 IN Catalytic Activities of Ligand H_2L^1 with the Addition of Divalent Metal Ions (M^{2+}) in Solution

	3′-processing IC_{50} (μM)	strand transfer IC_{50} (μM)	SI[a]
$H_2L^1 + (Ni^{2+})$	320	57	6
$H_2L^1 + (Co^{2+})$	85	84	1
$H_2L^1 + (Cu^{2+})$	235	46	5
$H_2L^1 + (Zn^{2+})$	>333	40	>8

[a] SI = selectivity index.

Finally, we sought to understand if the activities of compound H_2L^1 and **9b** were influenced by the addition of the exogenous soft metal Co^{2+} due to the better activity of **9d** (Figure 7; **9b** has been chosen since Mn^{2+} is used in enzyme assays). Results revealed that ligand H_2L^1 showed an increase in potency with exogenous Co^{2+} in the reaction buffer only for 3′-processing (Table 6) as observed above, with the same anti-IN activity for ST. Interestingly, **9b** displayed an increase in inhibitory selectivity toward the strand transfer process when exogenous Co^{2+} was added to the reaction buffer (IC_{50} = <12 and >333 μM for ST and 3′-processing, respectively). A possible explanation for this result is that **9b** could in part coordinate another ion (Co^{2+}) in solution, thereby creating a species (polymetal complexes?) with a favorable combination of two different ions (Mn^{2+} and Co^{2+}) into the complex for IN strand transfer inhibition.

Do Diketo Acids Inhibit IN as Complexes? We attempted to rationalize the obtained results in order to clarify the mode of action of diketo acids. First, it was interesting to consider whether structural features of the prepared complexes correlated

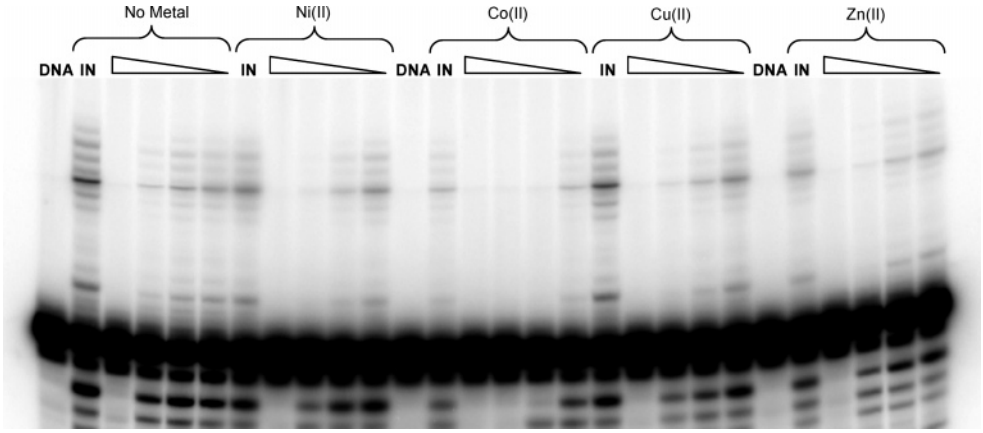

Figure 6. Inhibition of purified IN by H_2L^1 in decreasing concentrations (1 mM → 333 μM → 111 μM → 37 μM) before and after addition of exogenous metal to the reaction buffer, at IC_{50} concentration for 3′-processing, as observed in complex-related compounds and doubled since two metals can be coordinated: that is, Ni^{2+} (**9c**), 132 μM; Co^{2+} (**9d**), 100 μM; Cu^{2+} (**9e**), 52 μM; and Zn^{2+} (**9f**), 176 μM. Mn(II) is still present.

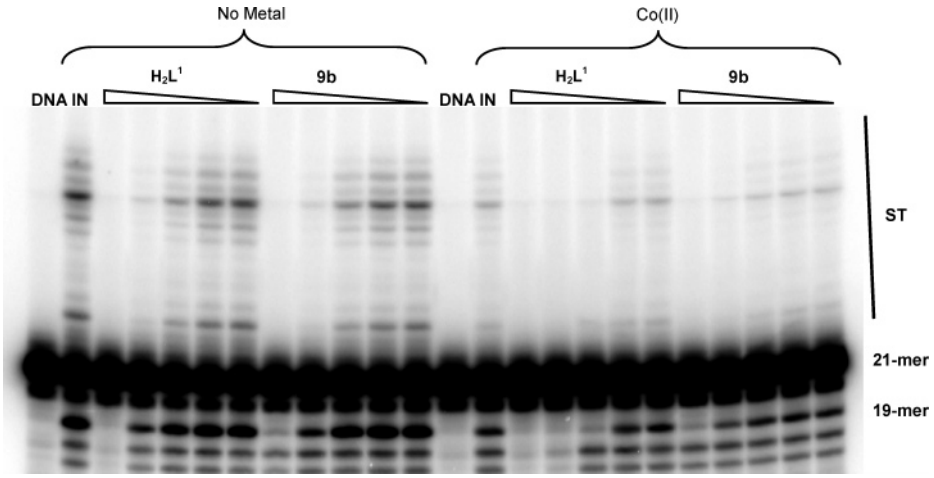

Figure 7. Same setup as in Figure 6 with both inhibitors H_2L^1 and **9b** at decreasing concentrations (1 mM → 333 μM → 111 μM → 37 μM → 12 μM) and exogenous Co^{2+} (100 μM) in the reaction buffer.

Table 6. Inhibition of HIV-1 IN Catalytic Activities of Ligand H_2L^1 and Complex **9b** in Assay Conditions (with Mn^{2+}) and after Addition of Exogenous Co^{2+}

compd	solution conditions	3′-processing IC_{50} (μM)	strand transfer IC_{50} (μM)	SI[a]
H_2L^1	no exogenous metal	>333	69 ± 4	5
9b	no exogenous metal	>333	42 ± 4	>8
H_2L^1	exogenous Co^{2+}	82 ± 3	80 ± 4	1
9b	exogenous Co^{2+}	>333	<12	>28

[a] SI = selectivity index.

with their anti-IN activities. Because at pH 7.5 the prevalent formation of species $[Mg_2L^1]^{2+}$ is promoted from H_2L^1, and MgL^3 (Mg_2L_2) from H_2L^3 (see potentiometry section), these species are expected to exist at physiological conditions. All **9a**−**f** and **11a**−**f** series of compounds are isolated in 1:1 metal−ligand complexes as minimum stoichiometry. While the stoichiometry of complexes in the **11** series (ML^3) could correspond to that found to be predominant at physiological pH for H_2L^3 in solution, the components of series **9** (ML^1) do not correspond to the species preferentially formed by H_2L^1 in solution at pH = 7.5 ($[M_2L]^{2+}$). Inhibition activities seem to confirm this assumption for complexes **11**. Additionally, we also prepared and tested complex **13** ($[Mg_2L^1]^{2+}$, the prevalent species at pH 7.5), obtained as a nitrate salt, to compare its anti-IN activity with that of free ligand H_2L^1. Interestingly, **13** and H_2L^1 showed comparable anti-IN activities (IC_{50} ST = 88 ± 5 for **13** versus 69 ± 6 for H_2L^1, with >333 μM for 3′-processing for each compound), thus suggesting that $[M_2L^1]^{2+}$ can be the "active species" of H_2L^1 in physiological and assay conditions. Moreover, the complexes **11a** (MgL^3) and **11b** (MnL^3) would constitute the species formed by H_2L^3 in the presence of Mg^{2+} or Mn^{2+} as metal cofactors. In summary, complexes $[M_2L^1]^{2+}$ and ML^3 could represent the "active species" of compounds **9a**−**f** and **11a**−**f**, respectively. At this stage, results indicate that the optimal metal−ligand combination can be attributed to compounds that act in the ML form. This result could represent a key finding to explain why compounds that have similar physicochemical properties show such great differences in inhibitory activities.

The formation of different species could not be simply related to the steric hindrance of the aryl substituent of the diketo acid's moiety, as discussed for the ligands H_2L^3 (see in the potentiometry section). The molecular basis to understand this behavior can be offered by correlating the differences in pK_as, presented from both ligands with their complexing abilities, to their inhibition activities. The importance of the aromatic framework could be attributed to its electronic influence on the β-diketo moiety, which directly affects the acidic constant values, one of the most important parameters involved in complex formation. Therefore, the diketo acids suitable to form ML (M_2L_2) species proved to be the better ligands.

Regarding the diketo esters, the species such as ML^+ (1:1) and ML_2 (1:2) are detected by potentiometric measurements in equimolar ratio. Because complexes **10** and **12** are constituted

in the 1:2 metal−ligand ratio, the steric hindrance of ML_2 could play a major role to explain the inhibitory activity of the more potent diketo ester **12**.

In the next step, these complexes may act as interfacial inhibitors by interfering with IN and acceptor DNA as proposed. In particular, they may block the strand transfer reaction by binding at the interface of IN and substrate DNA. However, a mimic-like interference ability of these complexes with respects to the transition state in the "two-metal dependent" phosphoryl-transfer mechanism of IN should also be considered.

Conclusion

We have demonstrated the metal complexing ability of diketo acids in solution, which directed us in the design and synthesis of new diketo acid complexes. These findings could be extended to other structurally related components of the diketo acid family such as 5CITEP, S-1360, and L-870,810. To better understand the biological profile of diketo acids, there are other questions that should be addressed. For example, why do certain diketo acid compounds that have similar physicochemical properties share different antiviral potency, with very few diketo acids showing antiviral activity at all? In fact, while H_2L^3 (L-731,-988) inhibits HIV-1 replication in cell-based assays, H_2L^1 is ineffective against HIV-1 replication. Because a prerequisite for the strand transfer activity is an efficient nuclear uptake, this should have a similar importance for antiviral activity. A possible explanation may be linked to the lipophilicity of the respective complexes, as shown by our results. In fact the species Mg_2L^{2+}, derived from H_2L^1, is predicted to be less lipophilic than the species MgL (M_2L_2), which was formed by H_2L^3. This lipophilic balance of complexes could play a key role in antiviral potency. Our study indicates that formation of such complexes could constitute a new strategy in discovering novel prototypes of IN inhibitors. Additionally, it is of major interest to define the role of diketo acids in their selectivity for the strand transfer catalytic reaction. Work is ongoing in this direction to build on the above-mentioned results and to perform further studies in this field.

Experimental Section

Chemistry: (A) For Ligands H_2L^{1-4} (1−4). Anhydrous solvents and all reagents were purchased from Aldrich, Merck, or Carlo Erba. All reactions involving air- or moisture-sensitive compounds were performed under nitrogen atmosphere, with oven-dried glassware and syringes used to transfer solutions. Melting points (mp) were determined on an Electrothermal or a Köfler apparatus and are uncorrected. Infrared (IR) spectra were recorded as thin films or Nujol mulls on NaCl plates with a Perkin-Elmer 781 IR spectrophotometer and are expressed as ν (cm^{-1}). Nuclear magnetic resonance (^1H NMR, ^{13}C NMR, and DEPT) spectra were determined in $CDCl_3$, DMSO-d_6, or $CDCl_3$/DMSO-d_6 (3:1 ratio) on a Varian XL-200 (200 MHz) or VXR-300 (300 MHz) spectrometer. Chemical shifts (δ scale) are reported in parts per million (ppm) downfield from tetramethylsilane (TMS) used as an internal standard. The assignment of exchangeable protons (O*H* and N*H*) was confirmed by the addition of D_2O. Electron ionization mass spectra (70 eV) were recorded on a Hewlett-Packard 5989 mass engine spectrometer. Analytical thin-layer chromatography (TLC) was done on Merck silica gel F-254 plates. For flash chromatography, Merck silica gel 60 was used with a particle size of 0.040−0.063 mm (230−400 mesh ASTM). Elemental analyses were performed on a Perkin-Elmer 2400 instrument at Laboratorio di Microanalisi, Dipartimento di Chimica, Università di Sassari (Italy); all values are given as percentages, and the results were within ±0.4% of the theoretical values.

(B) For Complexes 9−13. All reagents of commercial quality were used without further purification. Proton NMR spectra were recorded at 27 °C on a Bruker 300 FT spectrophotometer by using TMS as internal standard, while IR spectra were obtained with a Nicolet 5PCFT-IR spectrophotometer in the 4000−400 cm^{-1} range, using KBr disks or, where indicated, the reflectance mode on the powder. Elemental analyses were performed by using a Carlo Erba Model EA 1108 apparatus. Electrospray mass spectral analyses (ESI-MS) were performed on an Apex IV (7 T) Fourier transform ion cyclotron resonance instrument (FTICR) (Bruker Daltonics, Billerica, MA). Solutions were infused by syringe pump through the Apollo ESI source at 100 μL/h. Spectra were obtained from eight summed 0.5 s scans at the same source potentials for all samples.

General Procedure for the Preparation of Ligands β-Diketo Acids (1 and 3). A solution of the appropriate β-diketo ester (**2** or **4**) (1 mmol) in methanol (15 mL) was treated with 2 N NaOH (4 equiv) and stirred at room temperature for 5 h. After dilution with water, the reaction mixture was acidified with 1 N HCl. The white-beige (**1**) or yellow (**3**) precipitate that formed was filtered off, washed with water, and recrystallized from water/ethanol.

(2*Z*)-2-Hydroxy-4-oxo-4-phenylbut-2-enoic acid (1).[57] Yield 65%; mp 149−150 °C (decomp); IR (Nujol) ν (cm^{-1}) 1735 (C═O acid), 1625 (C═O ketone). ^1H NMR (300 MHz, $CDCl_3$ + DMSO-d_6) δ 14.50−13.40 (br s, 1H, OH), 8.01 (d, 2H, Ar−H), 7.66 (t, 1H, Ar−H), 7.55 (t, 2H, Ar−H), 7.09 (s, 1H, C═C−H); ^1H NMR (200 MHz, DMSO-d_6) δ 14.60−12.80 (br s, 1H, OH), 8.08 (d, 2H, Ar−H), 7.72 (t, 1H, Ar−H), 7.59 (t, 2H, Ar−H), 7.13 (s, 1H, C═C−H); ^{13}C NMR (50 MHz, DMSO-d_6) δ 190.4, 170.2, 163.2, 134.6, 134.1, 129.1, 127.9, 97.9. MS *m*/*z* 192 (M^+), 69 (base). Anal. ($C_{10}H_8O_4$) C, H.

(2*Z*)-4-[1-(4-Fluorobenzyl)-1*H*-pyrrol-2-yl]-2-hydroxy-4-oxobut-2-enoic Acid (3). Yield 68%, mp 164−6 °C (decomp); IR (Nujol) ν (cm^{-1}) 1707 (C═O acid), 1624 (C═O ketone). ^1H NMR (300 MHz, $CDCl_3$ + DMSO-d_6) δ 14.80−14.20 (br s, 1H, OH), 7.16−7.11 (m, 3H, Ar−H), 6.99 (t, 3H, Ar−H), 6.83 (s, 1H, C═C−H), 6.29 (dd, 1H, Ar−H), 5.61 (s, 2H, CH_2); ^1H NMR (200 MHz, DMSO-d_6) δ 14.60−13.20 (br s, 1H, OH), 7.55−7.53 (m, 1H, Ar−H), 7.44−7.42 (m, 1H, Ar−H), 7.23−7.05 (m, 4H, Ar−H), 6.86 (s, 1H, C═C−H), 6.33 (dd, 1H, Ar−H), 5.63 (s, 2H, CH_2); ^{13}C NMR (50 MHz, DMSO-d_6) δ 184.0, 163.8, 161.4, 134.3, 128.8, 128.7, 128.4, 122.1, 115.5, 115.1, 110.2, 101.0, 51.3. MS *m*/*z* 288 (M^+), 109 (base). Anal. ($C_{15}H_{12}FNO_4$) C, H, N.

General Procedure for the Preparation of Ligands β-Diketo Esters (2 and 4). To a solution of the appropriate acetyl derivative (**5** or **6**) (83.23 mmol) and dimethyl oxalate (99.92 mmol) in DMF (80 mL) was added NaH (60% oil dispersion, 100 mmol) at 5 °C. The mixture was stirred at room temperature for 3.5 h and then heated at 50 °C for 1 h. After the mixture was cooled in an ice−water bath, water was added and the resulting mixture was acidified with 3 N HCl to give a solid residue. The latter was collected, washed several times with water, and then recrystallized from water/ethanol to give **2** and **4** as white/beige and yellow crystals, respectively.

Methyl (2*Z*)-2-Hydroxy-4-oxo-4-phenylbut-2-enoate (2).[55,57] Yield 61%; mp 56−8 °C; IR (Nujol) ν (cm^{-1}) 1739 (C═O ester), 1631 (C═O ketone). ^1H NMR (300 MHz, $CDCl_3$) δ 15.30 (br s, 1H, OH), 8.00 (d, 2H, Ar−H), 7.61 (t, 1H, Ar−H), 7.51 (m, 2H, Ar−H), 7.10 (s, 1H, C═C−H), 3.95 (s, 3H, OCH_3); ^1H NMR (200 MHz, DMSO-d_6) δ 14.90−14.10 (br s, 1H, OH), 8.07 (d, 2H, Ar−H), 7.71 (t, 1H, Ar−H), 7.58 (m, 2H, Ar−H), 7.11 (s, 1H, C═C−H), 3.87 (s, 3H, OCH_3); ^{13}C NMR (50 MHz, $CDCl_3$) δ 190.8, 169.2, 162.7, 134.8, 133.8, 128.9, 127.9, 98.0, 53.2; ^{13}C NMR (50 MHz, DMSO-d_6) δ 190.2, 168.6, 162.1, 134.4, 134.1, 129.1, 127.9, 98.1, 53.1. MS *m*/*z* 206 (M^+), 69 (base). Anal. ($C_{11}H_{10}O_4 \cdot 0.25H_2O$) C, H.

Methyl (2*Z*)-4-[1-(4-Fluorobenzyl)-1*H*-pyrrol-2-yl]-2-hydroxy-4-oxobut-2-enoate (4).[56] Yield 68%; mp 103−5 °C; IR (Nujol) ν (cm^{-1}) 1726 (C═O ester), 1623 (C═O ketone). ^1H NMR (300 MHz, $CDCl_3$ + DMSO-d_6) δ 14.51 (br s, 1H, OH), 7.15−7.09 (m, 3H, Ar−H), 6.99 (t, 3H, Ar−H), 6.85 (s, 1H, C═C−H), 6.30−6.27 (m, 1H, Ar−H), 5.60 (s, 2H, CH_2), 3.91 (s, 3H, OCH_3); ^1H NMR (200 MHz, DMSO-d_6) δ 14.80−13.60 (br s, 1H, OH), 7.57 (s, 1H,

Ar−H), 7.48−7.45 (m, 1H, Ar−H), 7.22−7.10 (m, 4H, Ar−H), 6.89 (s, 1H, C═C−H), 6.36−6.33 (m, 1H, Ar−H), 5.62 (s, 2H, CH_2) 3.82 (s, 3H, OCH_3); ^{1}H NMR (200 MHz, $CDCl_3$) δ 14.50 (br s, 1H, OH), 7.15−6.94 (m, 6H, Ar−H), 6.86 (s, 1H, C═C−H), 6.84 (s, 1H, Ar−H), 6.30−6.26 (m, 1H, Ar−H), 5.59 (s, 2H, CH_2), 3.90 (s, 3H, OCH_3); ^{13}C NMR (50 MHz, DMSO-d_6) δ 183.6, 163.8, 162.3, 160.0, 134.7, 134.6, 128.8, 128.6, 128.3, 122.5, 115.5, 115.0, 110.3, 101.3, 52.8, 51.3; ^{13}C NMR (50 MHz, $CDCl_3$) δ 184.3, 164.6, 163.0, 160.2, 133.4, 132.5, 129.2, 128.8, 128.6, 121.3, 115.7, 115.3, 110.1, 101.7, 52.9, 52.2. MS *m*/*z* 303 (M^+), 109 (base). Anal. ($C_{16}H_{14}FNO_4$) C, H, N.

Preparation of 1-[1-(4-Fluorobenzyl)-1*H*-pyrrol-2-yl]ethanone (6).[56] A mixture of KOH (crushed pellets) (4 equiv) in DMSO (18 mL) was stirred at room temperature for 5 min. 2-Acetylpyrrole **7** (9.0 mmol) was added and the mixture was stirred for 45 min. After this time, 4-fluorobenzylbromide was added (2 equiv) and the reaction mixture was stirred at room temperature for a further 45 min. The reaction was then quenched by the addition of water and the solution was extracted three times with diethyl ether. The combined organic layers were washed with water and dried over Na_2SO_4. After evaporation of the solvent, the residue was purified by silica gel flash chromatography (eluents petroleum ether−ethyl acetate 9:1) to give an yellow oil. Yield 94%; mp, oil at room temperature; IR (Nujol) ν (cm^{-1}) = 1640 (ketone). ^{1}H NMR (200 MHz, $CDCl_3$) δ 7.36−7.28 (m, 2H, Ar−H), 7.11−6.83 (m, 4H, Ar−H), 6.22−6.18 (m, 1H, Ar−H), 5.53 (s, 2H, CH_2), 2.41 (s, 3H, $COCH_3$). MS *m*/*z* 217 (M^+).

Preparation of 1-(1*H*-Pyrrol-2-yl)ethanone (7).[56] A solution of 2-acetylfuran **8** (45 mmol) and 30% NH_3 (19 equiv) in 96% ethanol (30 mL) was heated in a sealed tube at 150 °C for 12 h. After cooling, the solution was filtered and concentrated in vacuo to give a brown solid. The latter was purified by silica gel flash chromatography (eluents petroleum ether−ethyl acetate 8:2) to give a yellow solid, which was recrystallized from H_2O/EtOH. Yield 75%; mp 88−89 °C; IR (Nujol) ν (cm^{-1}) = 3260 (NH), 1640 (ketone). ^{1}H NMR (200 MHz, $CDCl_3$) δ 10.50−9.80 (br s, 1H, NH), 7.06−7.04 (m, 1H, Ar−H), 6.93−6.91 (m, 1H, Ar−H), 6.28−6.26 (m, 1H, Ar−H), 2.45 (s, 3H, $COCH_3$). MS *m*/*z* 109 (M^+).

Preparation of Complexes 9a−f, 10, 11a−f, 12, and 13: $MgL^1\cdot 3H_2O$ (9a). A suspension of magnesium hydroxide (75 mg, 1.3 mmol) in water (10 mL) was added to a methanolic solution (15 mL) of H_2L^1 (250 mg, 1.3 mmol). The reaction mixture was stirred at room temperature overnight and then filtered. After concentration of the solution, a white powder was isolated. Yield 45%; mp >250 °C. IR (cm^{-1}) $\nu_{C=O}$ = 1607, 1576. ^{1}H NMR (CD_3OD) δ 8.01−7.88 (m, 2H), 7.54−7.45 (m, 3H), 7.10 (s, 1H, HC═C). Anal. Calcd for $C_{10}H_6O_4Mg\cdot 3H_2O$.

$MnL^1\cdot H_2O$ (9b). An aqueous solution (10 mL) of $Mn(CH_3COO)_2\cdot 4H_2O$ (255 mg, 1 mmol) was added to a methanolic solution (10 mL) of H_2L^1 (200 mg, 1 mmol) and a yellow powder immediately precipitated. This was stirred at room temperature for an additional 2 h and then filtered off and washed with methanol and water. Yield 94%; mp >250 °C. IR (cm^{-1}) $\nu_{C=O}$ = 1594, 1570. ESI-MS *m*/*z* 282 [($MnL^1 + 2H_2O + H)^+$], 354 [($MnL^1 + 6H_2O + H)^+$]. Anal. ($C_{10}H_6O_4Mn\cdot H_2O$) C, H.

The same procedure was followed with the acetates of the other metals.

$NiL^1\cdot 2.5H_2O$ (9c). Green powder; yield 96%; mp >250 °C. IR (cm^{-1}) $\nu_{C=O}$ = 1595, 1571. Anal. ($C_{10}H_6O_4Ni\cdot 2.5H_2O$) C, H.

$CoL^1\cdot 2H_2O$ (9d). Orange powder; yield 95%; mp >250 °C. IR (cm^{-1}) $\nu_{C=O}$ = 1594, 1569. Anal. ($C_{10}H_6O_4Co\cdot 2H_2O$) C, H.

$CuL^1\cdot 0.5H_2O$ (9e). Green powder; yield 46%; mp >250 °C. IR (cm^{-1}) $\nu_{C=O}$ = 1662, 1592, 1567. Anal. ($C_{10}H_6O_4Cu\cdot 0.5H_2O$) C, H.

$ZnL^1\cdot H_2O$ (9f). White powder; yield 44%; mp >250 °C. IR (cm^{-1}) $\nu_{C=O}$ = 1595, 1572. ^{1}H NMR (DMSO-d_6) δ 7.91 (br d, 2H), 7.59−7.47 (m, 3H); 7.09 (br m, 1H, HC═C). Anal. ($C_{10}H_6O_4Zn\cdot H_2O$) C, H.

$Mg(L^2)_2\cdot 2H_2O$ (10). A suspension of magnesium hydroxide (35 mg, 0.6 mmol) in water (10 mL) was added to a methanolic solution (15 mL) of HL^2 (250 mg, 1.2 mmol). After few minutes a white powder precipitated. This was stirred at room temperature for 1 h and then filtered off and washed with methanol. Yield 88%; mp 161−163 °C (decomp). IR (cm^{-1}) ν_{OH} = 3447; $\nu_{C=O}$ = 1733, 1615, 1576. ^{1}H NMR (CD_3OD) δ 7.87 (d, 2H), 7.40−7.28 (t + d, 3H), 6.69 (s, 1H, HC═C). FAB-MS *m*/*z* 435 [($Mg(L^2)_2 + H)^+$], 663 [$Mg_2(L^2)_3^+$]. Anal. ($C_{22}H_{18}O_8Mg\cdot 2H_2O$) C, H.

The complexes of H_2L^3 are obtained as the corresponding complexes of H_2L^1.

$MgL^3\cdot 2H_2O$ (11a). After the mixture was stirred overnight at room temperature, the solvent was removed and the crude product was dissolved in CH_2Cl_2. A white powder precipitated, which was filtered off, washed with dichloromethane, and dried under vacuum. Yield 45%; mp 150 °C (decomp). IR (cm^{-1}) $\nu_{C=O}$ = 1585. ^{1}H NMR (CD_3OD) δ 7.22−6.95 (m, 7H, arom + CH_{imid} + CH_{enolic}), 6.24 (br s, 1H, CH_{imid}), 5.60 (s, 2H, CH_2). ESI-MS *m*/*z* 348 [($MgL^3 + 2H_2O + H)^+$]. Anal. ($C_{15}H_{10}FNO_4Mg\cdot 2H_2O$) C, H, N.

$MnL^3\cdot H_2O$ (11b). Yellow powder; yield 80%; mp >250 °C. IR (cm^{-1}) $\nu_{C=O}$ = 1577. ESI-MS *m*/*z* 379 [($MnL^3 + 2H_2O + H)^+$]. Anal. ($C_{15}H_{10}FNO_4Mn\cdot H_2O$) C, H, N.

$NiL^3\cdot H_2O$ (11c). Pale green powder; yield = 82%; mp >250 °C. IR (cm^{-1}) $\nu_{C=O}$ = 1576. ESI-MS *m*/*z* 326 [($NiL^3 - F)^+$]; 364 [($NiL^3 + H_2O + H)^+$]; 434 [($NiL^3 + 6H_2O - F)^+$]. Anal. ($C_{15}H_{10}FNO_4Ni\cdot H_2O$) C, H, N.

$CoL^3\cdot H_2O$ (11d). Orange powder; yield 96%; mp >250 °C. IR (cm^{-1}) $\nu_{C=O}$ = 1583. ESI-MS *m*/*z* 471 [($CoL^4 + 8H_2O - F)^+$]. Anal. ($C_{15}H_{10}FNO_4Co\cdot H_2O$) C, H, N.

$CuL^3\cdot 1.5H_2O$ (11e). Green powder; yield 62%; mp >250 °C. IR (cm^{-1}) $\nu_{C=O}$ = 1662, 1591, 1567. ESI-MS *m*/*z* 391 [($CuL^3 + H_2O + Na)^+$]. Anal. ($C_{15}H_{10}FNO_4Cu\cdot 1.5H_2O$) C, H, N.

$ZnL^3\cdot 0.5H_2O$ (11f). Light yellow powder; yield 67%; mp >250 °C. IR (cm^{-1}) $\nu_{C=O}$ = 1580. Anal. ($C_{15}H_{10}FNO_4Zn\cdot 0.5H_2O$) C, H, N.

$Mg(L^4)_2\cdot 2H_2O$ (12). Ligand HL^4 (0.1 g, 0.3 mmol) was dissolved in 15 mL of methanol, and a solution of 10 mg (0.015 mmol) of $Mg(OH)_2$ dispersed in 10 mL of water was added. Immediately after the addition of the metal salt, a light yellow powder precipitated. This was stirred at room temperature for an additional 2 h and then filtered off and washed with diethyl ether. Yield 65%; mp 95−97 °C. IR (cm^{-1}) ν_{OH} = 3441; $\nu_{C=O}$ = 1727, 1631, 1583. ^{1}H NMR (CD_3OD) δ 7.12−6.97 (m, 4H), 6.78 (t, 2H, CH_{imid}), 6.47 (s, 1H, CH_{enolic}), 6.12 (br t, 1H, CH_{imid}), 5.45 (s, 2H, CH_2), 3.74 (s, 3H, OCH_3). FAB-MS *m*/*z* 629 [($Mg(L^4)_2 + H)^+$]; 954 [$Mg_2(L^4)_3^+$]. Anal. ($C_{32}H_{26}F_2N_2O_8Mg\cdot 2H_2O$) C, H, N.

$[Mg_2L^1](NO_3)_2$ (13). H_2L^1 (0.1 g, 0.5 mmol) was dissolved in 15 mL of methanol and water (1:1) with the pH adjusted to 7 by using a 0.1 M aqueous solution of NaOH. The ligand was then added dropwise to an aqueous solution of $Mg(NO_3)_2$ (1 mmol). The reaction mixture was stirred at room temperature for 2 h and the solvent was removed under vacuum. The residue was retrieved with methanol, filtered, and concentrated. Upon removal of the solvent, a highly hygroscopic white powder was isolated. The hygroscopic nature of the product prevented the determination of elemental analysis. IR (reflectance mode, cm^{-1}) $\nu_{C=O}$ = 1631; ν_{NO_3} = 1345. ^{1}H NMR (CD_3OD) δ 8.05 (d, 2H), 7.65 (t, 1H), 7.54 (t, 2H), 7.14 (s, 1H, HC═C). ESI-MS *m*/*z* 300 [($Mg_2L^1(NO_3)^+$], 336 [($Mg_2L^1(NO_3) + 2H_2O)^+$], 399 [($Mg_2L^1(NO_3)_2 + H)^+$].

X-ray Crystallography. Crystals of H_2L^3 suitable for X-ray diffraction were obtained by slow evaporation of a water/acetic acid solution (50/50 v/v) of the ligand. Single-crystal X-ray diffraction analysis was carried out at room temperature on a computer-controlled Siemens AED diffractometer with Cu Kα (λ = 1.541 78 Å). No crystal decay was observed. The intensity data were processed with a peak-profile analysis procedure and corrected for Lorentz and polarization effects. The phase problem was solved by direct methods, by use of SIR 97.[63] Full-matrix least-squares refinements were carried out with SHELXS 97,[64] implemented in the WinGX package.[65] Analyses of the extinction and intensity statistics indicate that H_2L^3 crystallizes in space group $P2_1$, with two independent molecules in the asymmetric unit, related by a pseudo inversion center situated at (1, 0, $^3/_4$). Anisotropic thermal displacement parameters were refined for all non-H atoms. All H

atoms were distinguished by Fourier maps and refined isotropically. The Cambridge Crystallographic Database[66] software and PARST95[67] were used for analyzing and drawing the molecular structures. Detailed analyses are listed in Tables 1 and 2.

Potentiometric Measurements. Equilibrium constants for protonation and complexation reactions were determined by means of potentiometric measurements, carried out in methanol/water = 9:1 (v/v) solution at ionic strength 0.1 M KCl and 25 ± 0.1 °C, in the pH range 2.5−11 under N_2. Temperature was controlled to ±0.1 °C by use of a thermostatic circulating water bath (Isco GTR 2000 IIx). Appropriate aliquots of ligand solution, prepared by weight, were titrated with standard KOH (methanol/water = 9:1 (v/v), I = 0.1 M KCl) with and without Mg^{2+} ions. Constant-speed magnetic stirring was applied throughout. Freshly boiled methanol and double-distilled water, kept under N_2, were used throughout. The experimental procedure for determination of accurate equilibrium constants in this mixed solvent has been described in detail.[68] The protonation constants of the ligands were obtained by titrating 20−50-mL samples of each ligand (5×10^{-3} to 7×10^{-3} M). For the complex formation constants, the titrations were performed with different ligand/metal ratios (1 up to 4). At least two measurements (about 80 experimental points in each) were performed for each system. Potentiometric titrations were carried out by a fully automated apparatus equipped with a Crison GLP 21−22 digital voltmeter (resolution 0.1 mV) and a 5 mL Metrohm Dosimat 655 autoburet, both controlled by in-house software, written in BASIC, working on an IBM computer. The electrodic chain (Crison 5250 glass electrode and KCl 0.1 M in methanol/water = 9:1 (v/v) calomel electrode, Radiometer 401) was calibrated in terms of $[H^+]$ by means of a strong acid−strong base titration, by the method of Gran,[69] allowing the determination of the standard potential, E_o (373.7 ± 0.1 mV) and of the ionic product of water, K_w (pK_w = 14.38 ± 0.01) in the experimental conditions used. The software HYPERQUAD[70] was used to evaluate the protonation and complexation constants from emf data.

Biological Materials, Chemicals, and Enzymes. All compounds were dissolved in DMSO and the stock solutions were stored at −20 °C. The [γ-^{32}P]ATP was purchased from either Amersham Biosciences or ICN. The expression system for wild-type IN was a generous gift of Dr. Robert Craigie, Laboratory of Molecular Biology, NIDDK, NIH, Bethesda, MD.

Preparation of Oligonucleotide Substrates. The oligonucleotides 21top, 5′-GTGTGGAAAATCTCTAGCAGT-3′, and 21bot, 5′-ACTGCTAGAGATTTTCCACAC-3′, were purchased from Norris Cancer Center Core Facility (University of Southern California) and purified by UV shadowing on polyacrylamide gel. To analyze the extent of 3′-processing and strand transfer by use of 5′-end labeled substrates, 21top was 5′-end-labeled with T_4 polynucleotide kinase (Epicenter, Madison, WI) and [γ-^{32}P]ATP (Amersham Biosciences or ICN). The kinase was heat-inactivated and 21bot was added in 1.5-fold molar excess. The mixture was heated at 95 °C, allowed to cool slowly to room temperature, and run through a spin 25 minicolumn (USA Scientific) to separate annealed double-stranded oligonucleotide from unincorporated material.

Integrase Assays. To determine the extent of 3′-processing and strand transfer, wild-type IN was preincubated at a final concentration of 200 nM with the inhibitor in reaction buffer [50 mM NaCl, 1 mM *N*-(2-hydroxyethylpiperazine-*N*′-2-ethanesulfonic acid (HEPES), pH 7.5, 50 μM ethylenediaminetetraacetic acid (EDTA), 50 μM dithiothreitol, 10% glycerol (w/v), 7.5 mM $MnCl_2$, 0.1 mg/mL bovine serum albumin, 10 mM 2-mercaptoethanol, 10% DMSO, and 25 mM 3-(*N*-morpholino)propanesulfonic acid (MOPS, pH 7.2) at 30 °C for 30 min. For exogenous metal experiments, the salt ($NiSO_4$, $CoSO_4$, $CuCl_2$, and $ZnCl_2$) of each "soft" metal was added to the reaction buffer to give a final concentration that corresponded to the 3′-processing IC_{50} value of the analogous metal complex (**9c−f**). Then, 20 nM of the 5′-end ^{32}P-labeled linear oligonucleotide substrate was added, and incubation was continued for an additional 1 h. Reactions were quenched by the addition of an equal volume (16 μL) of loading dye (98% deionized formamide, 10 mM EDTA, 0.025% xylene cyanol, and 0.025% bromophenol blue). An aliquot (5 μL) was electrophoresed on a denaturing 20% polyacrylamide gel (0.09 M Tris−borate, pH 8.3, 2 mM EDTA, 20% acrylamide, and 8 M urea).

Gels were dried, exposed in a PhosphorImager cassette, analyzed on a Typhoon 8610 variable-mode imager (Amersham Biosciences), and quantitated by ImageQuant 5.2. Percent inhibition (% I) was calculated from

$$\% I = 100 \times [1 - (D - C)/(N - C)]$$

where C, N, and D are the fractions of 21-mer substrate converted to 19-mer (3′-processing product) or strand transfer products for DNA alone, DNA plus IN, and IN plus drug, respectively. The IC_{50} values were determined by plotting the logarithm of drug concentration versus percent inhibition to obtain the concentration that produced 50% inhibition.

Acknowledgment. M.S. dedicates this work to the memory of Mrs. Grazia Farre. We thank Dr. Maria Orecchioni, Mr. Paolo Fiori for assistance with NMR spectroscopy, and Dr. Luciano Sannia and Ms. Maria Paola Delussu for their help on the preparation of the ligands. M.S. is grateful to Ministero dell'Istruzione, dell'Università e della Ricerca (MIUR), Rome, Italia, and to Professor Giuseppe Paglietti for the partial financial support. The work in N.N.'s laboratory was supported by funds from the GlaxoSmithKline Drug Discovery Award. We thank the "Centro Interfacoltà Misure *Giuseppe Casnati*" and the "Laboratorio di Strutturistica *Mario Nardelli*" of the University of Parma for facilities.

Supporting Information Available: Distribution diagram for the ligands H_2L^1 and H_2L^3 and elemental analysis data for ligands and complexes. This material is available free of charge via the Internet at http://pubs.acs.org. Crystallographic data (excluding structure factors) for H_2L^3 have been deposited with the Cambridge Crystallographic Data Centre as Supplementary Publications No. CCDC 298663. Copies of the data can be obtained free of charge on application to CCDC, 12 Union Road, Cambridge CB2 1EZ, U.K. [fax (+44) 1223-336-033; e-mail deposit@ccdc.cam.ac.uk].

References

(1) De Clercq, E. Strategies in the design of antiviral drugs. *Nat. Rev. Drug Discovery* **2002**, *1*, 13−25.
(2) Turpin, J. A. The next generation of HIV/AIDS drugs: novel and developmental antiHIV drugs and targets. *Expert Rev. Anti-Infect. Ther.* **2003**, *1*, 97−128.
(3) De Clercq, E. New approaches toward anti-HIV chemotherapy. *J. Med. Chem.* **2005**, *48*, 1297−1313.
(4) Pommier, Y.; Neamati, N. Inhibitors of human immunodeficiency virus integrase. *Adv. Virus Res.* **1999**, *52*, 427−458.
(5) Neamati, N.; Marchand, C.; Pommier, Y. HIV-1 integrase inhibitors: past, present, and future. *Adv. Pharmacol.* **2000**, *49*, 147−165.
(6) Neamati, N. Structure-based HIV-1 integrase inhibitor design: a future perspective. *Expert Opin. Invest. Drugs* **2001**, *10*, 281−296.
(7) d'Angelo, J.; Mouscadet, J. F.; Desmaele, D.; Zouhiri, F.; Leh, H. HIV-1 integrase: the next target for AIDS therapy? *Pathol. Biol.* **2001**, *49*, 237−246.
(8) Anthony, N. J. HIV-1 integrase: a target for new AIDS chemotherapeutics. *Curr. Top. Med. Chem.* **2004**, *4*, 979−990.
(9) Pommier, Y.; Johnson A. A.; Marchand, C. Integrase inhibitors to treat HIV/ AIDS. *Nat. Rev. Drug Discovery* **2005**, *4*, 236−248.
(10) Richman, D. D. HIV chemotherapy. *Nature* **2001**, *410*, 995−1001.
(11) Barbaro, G.; Scozzafava, A.; Mastrolorenzo, A.; Supuran, C. T. Highly active antiretroviral therapy: current state of the art, new agents and their pharmacological interactions useful for improving therapeutic outcome. *Curr. Pharm. Des.* **2005**, *11*, 1850−1843.
(12) Cohen, J. Therapies. Confronting the limits of success. *Science* **2002**, *296*, 2320−2324.
(13) Little, S. J.; Holte, S.; Routy, J. P.; Daar, E. S.; Markowitz, M.; Collier, A. C.; Koup, R. A.; Mellors, J. W.; Connick, E.; Conway, B.; Kilby, M.; Wang, L.; Whitcomb, J. M.; Hellmann, N. S., Richman, D. D. Antiretroviral-drug resistance among patients recently infected with HIV. *New Engl. J. Med.* **2002**, *387*, 385−394.

(14) Engelman, A.; Mizuuchi, K.; Craigie, R. HIV-1 DNA integration: mechanism of viral DNA cleavage and DNA strand transfer. *Cell* **1991**, *67*, 1211−1221.
(15) Brown, P. O. *Integration*; Cold Spring Harbor Press: Cold Spring Harbor, NY, 1999.
(16) Asante-Appiah, E.; Skalka, A. M. HIV-1 integrase: structural organization, conformational changes, and catalysis. *Adv. Virus Res.* **1999**, *52*, 351−369.
(17) Steitz, T. A. A mechanism for all polymerases. *Nature* **1998**, *391*, 231−232.
(18) Dyda, F.; Hickman, A. B.; Jenkins, T. M.; Engelman, A.; Craigie, R.; Davies, D. R. Crystal structure of the catalytic domain of HIV-1 integrase: similarity to other polynucleotidyl transferases. *Science* **1994**, *266*, 1981−1986.
(19) Rice, P. A.; Baker, T. A. Comparative architecture of transposase and integrase complexes. *Nat. Struct. Biol.* **2001**, *8*, 302−307.
(20) Esposito, D.; Craigie, R. HIV integrase structure and function. *Adv. Virus Res.* **1999**, *52*, 319−333.
(21) Chiu, T. K.; Davies, D. R. Structure and function of HIV-1 integrase. *Curr. Top. Med. Chem.* **2004**, *4*, 671−686.
(22) Steitz, T. A. DNA polymerases: structural diversity and common mechanism. *J. Biol. Chem.* **1999**, *274*, 17395−17398.
(23) Horton, N. C., Perona, J. J. Making the most of metal ions. *Nat. Struct. Biol.* **2001**, *8*, 290−293.
(24) Feng, M.; Patel, D.; Dervan, J. J.; Ceska, T.; Suck, D.; Haq, I.; Sayers, J. R. Roles of divalent metal ions in flap endonuclease−substrate interactions. *Nat. Struct. Biol.* **2004**, *11*, 450−456.
(25) Grobler, J. A.; Stillmock, K.; Hu, B.; Witmer, M.; Felock, P.; Espeseth, A. S.; Wolfe, A.; Egbertson, M.; Bourgeois, M.; Melamed, J.; Wai, J. S.; Young, S.; Vacca, J.; Hazuda, D. J. Diketo acid inhibitor mechanism and HIV-1 integrase: Implications for metal binding in the active site of phosphotransferase enzymes. *Proc. Natl. Acad. Sci. U.S.A.* **2002**, *99*, 6661−6666.
(26) Marchand, C.; Johnson, A. A.; Karki, R. G.; Pais, G. C.; Zhang, X.; Cowansage, K.; Patel, T. A.; Nicklaus, M. C.; Burke, T. R., Jr.; Pommier, Y. Metal-dependent inhibition of HIV-1 integrase by beta-diketo acids and resistance of the soluble double-mutant (F185K/C280S). *Mol. Pharmacol.* **2003**, *64*, 600−609.
(27) Long, Y. Q.; Jiang, X. H.; Dayam, R.; Sanchez, T.; Shoemaker, R.; Sei, S.; Neamati, N. Rational design and synthesis of novel dimeric diketoacid-containing inhibitors of HIV-1 integrase: Implication for binding to two metal ions on the active site of integrase. *J. Med. Chem.* **2004**, *47*, 2561−2573.
(28) Lins, R. D.; Adesokan, A.; Soares, T. A.; Briggs, J. M. Investigations on human immunodeficiency virus type 1 integrase/DNA binding interactions via molecular dynamics and electrostatics calculations. *Pharmacol. Ther.* **2000**, *85*, 123−131.
(29) Neamati, N. Patented small molecule inhibitors of HIV-1 integrase: a ten-year saga. *Expert Opin. Ther. Pat.* **2002**, *12*, 709−724.
(30) Dayam, R.; Neamati, N. Small-molecule HIV-1 integrase inhibitors: the 2001−2002 update. *Curr. Pharm. Des.* **2003**, *9*, 1789−1802.
(31) Gupta, S. P.; Nagappa, A. N. Design and development of integrase inhibitors as anti-HIV agents. *Curr. Med. Chem.* **2003**, *10*, 1779−1794.
(32) Maurin, C.; Bailly, F.; Cotelle, P. Structure−activity relationship of HIV-1 integrase inhibitor−enzyme−ligand interaction. *Curr. Med. Chem.* **2003**, *10*, 1795−1810.
(33) Johnson, A. A.; Marchand, C.; Pommier, Y. HIV-1 integrase inhibitors: a decade of research and two drugs in clinical trial. *Curr. Top Med. Chem.* **2004**, *4*, 671−686.
(34) Pais, G. C. G.; Burke, T. R. Novel aryl diketo-containing inhibitors of HIV-1 integrase. *Drugs Future* **2002**, *27*, 1101−1111.
(35) Goldgur, Y.; Craigie, R.; Cohen, G. H.; Fujiwara, T.; Yoshinaga, T.; Fujishita, T.; Sugimoto, H.; Endo, T.; Murai, H.; Davies, D. R. Structure of the HIV-1 integrase catalytic domain complexed with an inhibitor: a platform for antiviral drug design. *Proc. Natl. Acad. Sci. U.S.A.* **1999**, *96*, 13040−13043.
(36) Hazuda, D. J.; Felock, P.; Witmer, M.; Wolfe, A.; Stillmock, K.; Grobler, J. A.; Espeseth, A.; Gabryelski, L.; Schleif, W.; Blau, C.; Miller, M. D. Inhibitors of strand transfer that prevent integration and inhibit HIV-1 replication in cells. *Science* **2000**, *287*, 646−650.
(37) Wai, J. S.; Egbertson, M. S.; Payne, L. S.; Fisher, T. E.; Embrey, M. W.; Tran, L. O.; Melamed, J. Y.; Langford, H. M.; Guare, J. P., Jr.; Zhuang, L.; Grey, V. E.; Vacca, J. P.; Holloway, M. K.; Naylor-Olsen, A. M.; Hazuda, D. J.; Felock, P. J.; Wolfe, A. L.; Stillmock, K. A.; Schleif, W. A.; Gabryelski, L. J.; Young, S. D. 4-Aryl-2,4-dioxobutanoic acid inhibitors of HIV-1 integrase and viral replication in cells. *J. Med. Chem.* **2000**, *43*, 4923−4926.
(38) Pluymers, W.; Pais, G.; Van Maele, B.; Pannecouque, C.; Fikkert, V.; Burke, T. R., Jr.; De Clercq, E.; Witvrouw, M.; Neamati, N.; Debyser, Z. Inhibition of HIV-1 integration by diketo derivatives. *Antimicrob. Agents Chemother.* **2002**, *46*, 3292−3297.
(39) Pais, G. C. G.; Zhang, X.; Marchand, C.; Neamati, N.; Cowansage, K.; Svarovskaia, E. S.; Pathak, V. K.; Tang, Y.; Nicklaus, M.; Pommier, Y.; Burke, T. R., Jr. Structure activity of 3-aryl-1,3-diketo-containing compounds as HIV-1 integrase inhibitors. *J. Med. Chem.* **2002**, *45*, 3184−3194.
(40) Marchand, C.; Zhang, X.; Pais, G. C. G.; Cowansage, K.; Neamati, N.; Burke, T. R., Jr.; Pommier, Y. Structural determinants for HIV-1 integrase inhibition by β-diketo acids. *J. Biol. Chem.* **2002**, *277*, 12596−12603.
(41) Sechi, M.; Derudas, M.; Dallocchio, R.; Dessi, A.; Bacchi, A.; Sannia, L.; Carta, F.; Palomba, M.; Ragab, O.; Chan, C.; Shoemaker, R.; Sei, S.; Dayam, R.; Neamati, N. Design and synthesis of novel indole β-diketo acid derivatives as HIV-1 integrase inhibitors. *J. Med. Chem.* **2004**, *47*, 5298−5310.
(42) Espeseth, A. S.; Felock, P.; Wolfe, A. Witmer, M.; Grobler, J.; Anthony, N.; Egbertson, M.; Melamed, J. Y.; Young, S.; Hamill, T.; Cole, J. L.; Hazuda D. J. HIV-1 integrase inhibitors that compete with the target DNA substrate define a unique strand transfer conformation for integrase. *Proc. Natl. Acad. Sci. U.S.A.* **2000**, *97*, 11244−11249.
(43) Yoshinaga, T. S.; Fujishita, T.; Fujiwara, T. In vitro activity of a new HIV-1 integrase inhibitor in clinical development. Presented at the 9th Conference on Retroviruses and Opportunistic Infections, Seattle, WA, 2002.
(44) Billich, A. S-1360 Shionogi-GlaxoSmithKline. *Curr. Opin. Invest. Drugs* **2003**, *4*, 206−209.
(45) Young, S. L-870,810: A potent antiviral HIV integrase inhibitor with potential clinical utility. Presented at the XIV International AIDS Conference, West Point, PA, 2002.
(46) Hazuda, D. J.; Young, S. D.; Guare, J. P.; Anthony, N. J.; Gomez, R. P.; Wai, J. S.; Vacca, J. P.; Handt, L.; Motzel, S. L.; Klein, H. J.; Dornadula, G.; Danovich, R. M.; Witmer, M. V.; Wilson, K. A. A.; Tussey, L.; Schleif, W. A.; Gabryelski, L. S.; Jin, L.; Miller, M. D.; Casimiro, D. R.; Emini, E. A.; Shiver, J. W. Integrase inhibitors and cellular immunity suppress retroviral replication in rhesus macaques. *Science* **2004**, *305*, 528−532.
(47) Witvrouw, M.; Van Maele, B.; Vercammen, J., Hantson, A.; Engelborghs, Y.; De Clercq, E.; Pannecouque, Debyser, Z. Novel inhibitors of HIV-1 integration. *Curr. Drug. Metab.* **2004**, *5*, 291−304.
(48) Cowan, J. A. *The Biological Chemistry of Magnesium*; VCH: New York, 1995; pp 1−23.
(49) Pemberton, I. K.; Buckle, M.; Buc, H. The metal ion-induced cooperative binding of HIV-1 integrase to DNA exhibits a marked preference for Mn(II) rather than Mg(II). *J. Biol. Chem.* **1996**, *271*, 1498−1506.
(50) Chen, I.-J. ; Neamati, N.; MacKerrel, A. D., Jr. Structure-based inhibitor design targeting HIV-1 integrase. *Curr. Drug Target Infect. Dis.* **2002**, *2*, 217−234.
(51) Hazuda, D. J.; Hastings, J. C.; Wolfe, A. L.; Emini, E. A. A novel assay for the DNA strand-transfer reaction of HIV-1 integrase. *Nucleic Acids Res.* **1994**, *22*, 1121−1122.
(52) Mazumder, A.; Neamati, N.; Sunder, S.; Owen, J.; Pommier, Y. Retroviral integrase: A novel target in antiviral development; basic in vitro assays with the purified enzyme. In *Methods in Cellular and Molecular Biology: Antiviral Evaluation*; Humana Press: Totowa, NJ, 1999.
(53) Marchand, C.; Neamati, N.; Pommier, Y. In vitro human immunodeficiency virus type 1 integrase assays. *Method Enzymol.* **2001**, *340*, 624−633.
(54) Debyser, Z.; Cherepanov, P.; Pluymers, W.; De Clercq, E. Assays for the evaluation of HIV-1 integrase inhibitors. *Methods Mol. Biol.* **2001**, *160*, 139−155.
(55) Tanaka, A.; Terasawa, T.; Hagihara, H., Sakuma, Y.; Ishibe, N., Sawada, M.; Takasugi, H.; Tanaka, H. Inhibitors of acyl-CoA: cholesterol *O*-acyltransferase. 2. Identification and structure−activity relationships of a novel series of *N*-alkyl-*N*-(heteroaryl-substituted benzyl)-*N*′-arylureas. *J. Med. Chem.* **1998**, *41*, 2390−2410.
(56) Sechi, M.; Sannia, L.; Carta, F.; Palomba, M.; Dallocchio, R.; Dessì, A.; Derudas, M.; Zawahir, Z.; Neamati, N. Design of novel bioisosteres of β-diketoacid inhibitors of HIV-1 integrase. *Antiviral Chem. Chemother.* **2005**, *16*, 41−61.
(57) Maurin, C.; Bailly, F.; Cotelle, P. Improved preparation and structural investigation of 4-aryl-4-oxo-2-hydroxy-2-butenoic acids and methyl esters. *Tetrahedron* **2004**, *60*, 6479−6486.
(58) Brecker, L.; Pogorevc, M.; Griengl, H., Steiner, W.; Kappe, T.; Ribbons, D, W. Synthesis of 2,4-diketoacids and their aqueous solution structures. *New J. Chem.* **1999**, *23*, 437−446.
(59) Rossotti, F. J. C.; Rossotti, H. *The determination of stability constants and other equilibrium constants in solution*; McGraw-Hill: New York, 1961; Chapt. 17.

(60) Gatehouse, B. M.; O'Connor, M. J. The crystal and molecular structure of racemic [bis(ethylenediamine)acetylpyruvato]cobalt(III) iodide monohydrate. *Acta Crystallogr.* **1976**, *B32*, 3145−3148.
(61) Kawai, H.; Kitano, Y.; Mutoh, M.; Hata, G. Synthesis, structure and antitumor activity of a new water-soluble platinum complex, (1*R*,2*R*-cyclohexanediamine-*N*,*N*′)[2-hydroxy-4-oxo-2-pentenoato(2-)-O2]-platinum(II). *Chem. Pharm Bull. (Tokyo)* **1993**, *41*, 357−361.
(62) Maurin, C.; Bailly, F., Buisine, E.; Vezin, H.; Mbemba, G.; Mouscadet, J. F.; Cotelle, P. Spectroscopic studies of diketoacids−metal interactions. A probing tool for the pharmacophoric distance in the integrase active site. *J. Med. Chem.* **2004**, *47*, 5583−5586.
(63) Altomare, A.; Cascarano, G.; Giacovazzo, C.; Guagliardi, A.; Burla, M. C.; Polidori G.; Camalli, M. *SIR*92 − a program for automatic solution of crystal structures by direct methods *J. Appl. Crystallogr*. **1994**, *27*, 435−436.
(64) Sheldrick G. M. SHELXL97. Program for the Refinement of Crystal Structures; University of Gottingen: Gottingen, Germany, 1997.
(65) Farrugia, L. J. *WinGX* suite for small-molecule single-crystal crystallography. *J. Appl. Crystallogr*. **1999**, *32*, 837−838.
(66) Allen, F. H.; Kennard, O.; Taylor, R. Systematic analysis of structural data as a research technique in organic chemistry. *Acc. Chem. Res*. **1983**, *16*, 146−153.
(67) Nardelli, M. *PARST*95 − an update to *PARST*: a system of Fortran routines for calculating molecular structure parameters from the results of crystal structure analyses. *J. Appl. Crystallogr*. **1995**, *28*, 659.
(68) Fisicaro, E.; Braibanti, A. Potentiometric titrations in methanol/water medium: Intertitration variability. *Talanta* **1988**, *35*, 769−774.
(69) Gran, G. Determination of the equivalence point in potentiometric titrations. Part II. *Analyst* **1952**, *77*, 661.
(70) Gans, P.; Sabatini, A.; Vacca, A. Investigation of equilibria in solution. Determination of equilibrium constants with the HYPERQUAD suite of programs. *Talanta* **1996**, *43*, 1739−1753.

JM060193M